

Silicon drift detectors as a tool for time-resolved fluorescence XAFS on low-concentrated samples in catalysis

Peter Kappen,^{a*} Larc Tröger,^a Gerhard Materlik,^a Christian Reckleben,^b Karsten Hansen,^b Jan-Dierk Grunwaldt^{c†} and Bjerne S. Clausen^c

^aHamburger Synchrotronstrahlungslabor HASYLAB at Deutsches Elektronen-Synchrotron DESY, Notkestrasse 85, Hamburg, Germany, ^bDESY-FEC, Notkestrasse 85, D-22603 Hamburg, Germany, and ^cHaldor Topsøe A/S, Nymøllevej 55, DK-2800 Kgs. Lyngby, Denmark. E-mail: peter.kappen@desy.de

A silicon drift detector (SDD) was used for *ex situ* and time-resolved *in situ* fluorescence X-ray absorption fine structure (XAFS) on low-concentrated catalyst samples. For a single-element and a seven-element SDD the energy resolution and the peak-to-background ratio were verified at high count rates, sufficient for fluorescence XAFS. An experimental set-up including the seven-element SDD without any cooling and an *in situ* cell with gas supply and on-line gas analysis was developed. With this set-up the reduction and oxidation of a zeolite supported catalyst containing 0.3 wt% platinum was followed by fluorescence near-edge scans with a time resolution of 10 min each. From *ex situ* experiments on low-concentrated platinum- and gold-based catalysts fluorescence XAFS scans could be obtained with sufficient statistical quality for a quantitative analysis. Structural information on the gold and platinum particles could be extracted by both the Fourier transforms and the near-edge region of the XAFS spectra. Moreover, it was found that with the seven-element SDD concentrations of the element of interest as low as 100 ppm can be examined by fluorescence XAFS.

Keywords: silicon drift detectors; time-resolved; fluorescence; XAFS; *in situ*; catalysis; low-concentrated; gold; platinum; catalysts.

1. Introduction

X-ray absorption fine-structure (XAFS) spectroscopy is a valuable tool for studying the local structural environment around an element of interest in a multi-component catalyst (Clausen *et al.*, 1998; Iwasawa, 1996; Prins & Koningsberger, 1988). Furthermore, electronic properties and valence states of the elements in the sample can be obtained. Most commonly, XAFS of catalyst samples is measured in a transmission experiment (Clausen *et al.*, 1998; Iwasawa, 1996; Prins & Koningsberger, 1988). However, this method is only applicable to concentrated heterogeneous catalysts, where the element of interest has a concentration of more than about 1 wt%. The concentration limit strongly depends on the energy of the absorption edge and on the absorption of the matrix atoms. In the case of low-concentrated samples, fluorescence XAFS is the preferred technique (Iwasawa, 1996; Jaklevic *et al.*, 1977), where the use of energy-dispersive fluorescence detectors allows most of the fluorescence lines of the different elements in the sample to be clearly identified.

† Present address: Laboratory for Technical Chemistry, ETH Höggerberg, HCI D125, 8093 Höggerberg, Switzerland.

Fluorescence XAFS has been applied to a variety of fields such as catalysis, biology, environmental chemistry, archeometry and geology (Iwasawa, 1996; Gautier *et al.*, 1996; Manceau *et al.*, 1996; Brown *et al.*, 1995; Leutenegger *et al.*, 2000, and references therein; Greegor *et al.*, 1997). In order to obtain high-quality data, in many of these systems the low concentration of the component or element of interest can be compensated by long data-acquisition times. However, this is not a viable procedure in the case of catalysis where *in situ* and time-resolved measurements are of particular interest. Some *in situ* studies using fluorescence XAFS on moderately low-concentrated heterogeneous catalyst systems (few %) are known (Thomas *et al.*, 1994; Sankar *et al.*, 1995; Shannon *et al.*, 1996, 1997; Chun *et al.*, 2001). However, only very few results at low concentrations (<1 wt%) have been reported up to now (e.g. Kappen *et al.*, 2001; Grunwaldt, Kappen, Basini & Clausen, 2001; Grunwaldt, Kappen, Hammershøi *et al.*, 2001; Yamagushi *et al.*, 2000). In the case of these systems, energy-dispersive fluorescence detectors with high-count-rate performance are of major advantage.

Silicon drift detectors (SDD) with an integrated junction field effect transistor (JFET) can handle high count rates (Strüder *et al.*, 1997; Strüder, Fiorini *et al.*, 1998). These detectors can be operated at several hundred thousand counts per second with an appropriate energy resolution (<300 eV), while Ge-based detectors usually show less energy resolution at these count rates [e.g. measurements with a five-element high-count-rate Ge detector (model PGP 5seg h.c. from DSG) gave, with a shaping time of 250 ns at a total count rate TCR \approx 150 kcounts s⁻¹ and $E = 5.9$ keV, an energy resolution of \sim 850 eV, where the corresponding detector pixel size was 100 mm²]. However, latest developments using digital signal processing electronics for a multi-element HP-Ge detector also led to a good energy resolution (390 eV at 15.77 keV) at high count rates (150 kcounts s⁻¹) (Farrow *et al.*, 1998). For a number of experimental environments a certain compactness of the detector system is required.

Progress has been made in the development of thermoelectrically instead of cryogenically cooled Ge-based detectors (Derbyshire *et al.*, 1999). Also in this case the development of the SDD opens up an alternative, because it does not need any cooling (however, its performance is enhanced when using a Peltier element for cooling). Ongoing progress in parallelization through monolithic multipixel design (Hansen & Tröger, 2000; Lechner *et al.*, 2001) will allow SDDs to cover large solid angles resulting in better counting statistics. This will give interesting opportunities for time-resolved studies on low-concentrated samples.

In this publication we report on the application of a seven-element SDD for the *in situ* and *ex situ* investigation of catalysts containing very low concentrations of noble metals. For this purpose the count-rate-dependent performance of a one-element and a seven-element SDD are also discussed and compared with a modern HP-Ge detector system.

2. Silicon drift detector

2.1. General

In order to detect fluorescence photons of the order of several keV, different approaches have been used. As a non-energy-dispersive detector, a device based on an ionization chamber has been applied by Lytle *et al.* (1984). It covers a large solid angle ($\sim 4\pi \times 10\%$) with simultaneously some reduction of signal contributions from elastic scattering of the incident X-ray beam. This detector is also applicable to fluorescence XAFS in the soft X-ray regime (Lytle *et al.*, 1984).

However, energy-dispersive detectors have important advantages compared with the ionization chambers, since a unique identification

of the fluorescence radiation from each of the elements in a sample becomes possible. Even in comparatively simple systems consisting of a heavy element in a light matrix, energy-dispersive detectors are highly advantageous, because the precise discrimination of the fluorescence of interest from other signals (*e.g.* from elastically scattered photons) results in a clear enhancement of the XAFS data quality.

Commonly, semiconductors (*e.g.* Si, Ge, HgI₂ or GaAs) are used as detector materials, and the basic idea of operating such a detector is to use it as a reversely biased diode (see *e.g.* Knoll, 1979). The resulting electrical field generated is homogeneous, similar to that of a standard flat capacitor, hence leading to a comparatively large capacitance. Since the noise level and energy resolution are closely related to the capacitance of the detection system, the relatively large capacitance limits the detector performance. These limits can be overcome, *e.g.* by a silicon drift detector.

Fig. 1 schematically shows a pie-chart view of an SDD. Through incidence of a photon $h\omega$ a charge cloud is generated in the n⁻-type silicon bulk. Application of appropriate voltages to the p⁺ entrance window, covering one entire side of the Si chip, and to the p⁺ ring structure on the other side forms an inhomogeneous electrical field in the detector chip. This forces the negative charges to drift to a very small readout anode. Such a concept of charge transport was first proposed by Gatti & Rehak (1984). Silicon technology allows to monolithically integrate a JFET at the centre of the active silicon area (*e.g.* Lechner *et al.*, 1996), where the anode is connected to the gate contact of the JFET. Both small readout anode and integrated JFET lead to a very low detector capacitance (<100 fF; Strüder, 2000; Strüder, Fiorini *et al.*, 1998), so that low noise and good energy resolution can be achieved. In addition, the charge-collecting time in the SDD is short (~100 ns; Strüder *et al.*, 1999; Strüder, Lechner & Leutenegger, 1998), resulting in high-count-rate capabilities (several 100 kcounts s⁻¹). Further descriptions of the silicon drift technique can be found by, for example, Lechner *et al.* (2001); Strüder (2000); Strüder *et al.* (1997, 1999); Strüder, Fiorini *et al.* (1998); Strüder, Lechner & Leutenegger (1998); Lechner *et al.* (1993, 1996); and Gatti & Rehak (1984).

2.2. SDD performance aspects: experimental

The performance of a fluorescence detector (including its subsequent electronic components such as amplifier, ADC *etc.*) can be evaluated, for instance, by means of the energy resolution and the peak-to-background ratio of a fluorescence line (*e.g.* Leřy *et al.*, 1999). The energy resolution (\propto FWHM) determines whether two fluorescence signals can be separated. The peak-to-background ratio (P/B) is a measure for the lower limit of concentration of a species which can be detected. Often P/B is defined as the peak maximum of

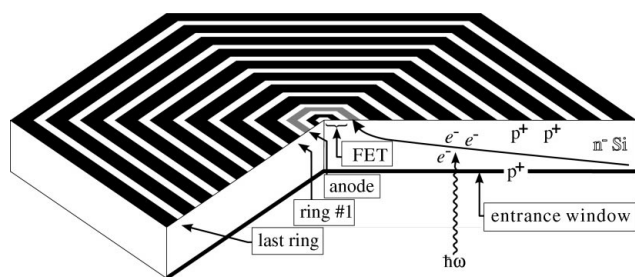


Figure 1
Schematic pie-chart view of one element of the used seven-element silicon drift detector [compare with Fig. 1 of Lechner *et al.* (1996) and Fig. 2 of Kappen, Grunwaldt *et al.* (2001)].

a fluorescence line divided by a mean background level in a certain energy interval (Lechner *et al.*, 2001; Leřy *et al.*, 1999; Strüder, 2000). This type of definition is dependent on the energy resolution of the detector and, since the background signal is mainly caused by incomplete charge collection in the sensitive detector volume, which does not affect the FWHM, we use a modified definition, $P/B :=$ (peak integral of fluorescence line)/(integrated background), leading to values that are no longer a function of the FWHM.

Experiments to measure the FWHM and P/B on a single-pixel SDD were carried out at the bending-magnet beamline X1 (Frahm, 1989; HASYLAB, 2001) at the synchrotron radiation facility Hamburger Synchrotronstrahlungslabor HASYLAB at Deutsches Elektronen-Synchrotron DESY. The detector was provided by KETEK GmbH, Munich. As a test fluorescence sample a Zn foil was irradiated with monochromatic radiation ($E = 10.5$ keV), using an Si(111) double-crystal monochromator. The incident photon flux was controlled *via* a monochromator-stabilizer (MoStab; Krolzig *et al.*, 1984), referring to an ionization chamber mounted between the monochromator and the sample. By detuning the monochromator crystals from parallel alignment, the number of photons on the Zn foil could be varied. The signal from the ionization chamber was used as a measure of the TCR incoming to the detector.

The detector was mounted perpendicular to the beam axis in order to minimize signals from elastic scattering. The output signals from the SDD were fed to a shaping amplifier (Silena 7611/L; shaping time 250 ns), and the number of incoming pulses was monitored *via* a fast counter (Canberra Dual Counter/Timer 1776). Since the amplifier works linearly for low count rates, the signal from the ionization chamber could be scaled to absolute units of TCR. An analog-to-digital converter (ADC, Silena 7423 UHS) was used to digitize the amplifier output signals, and the fluorescence spectra from the Zn sample were recorded by a multichannel analyzer (MCA, model MCD4LAP by FAST ComTec). The temperature of the SDD was varied using a Peltier element.

Analogous experiments were carried out for a seven-element SDD (SDD chip provided by KETEK GmbH, Munich) using a sample containing 1.8 wt% Ni in a matrix of 7.1 wt% Mo/Al₂O₃ as a fluorescing object. Each of the individual detector pixels has a sensitive area of 5 mm². The SDD chip is mounted in a metal housing, and it is covered by a light-tight entrance window (25 μ m Kapton foil evaporated with ~100 nm Al), since it is sensitive towards visible light. Seven independent pre-amplifiers and shaper channels (shaping time 280 ns) are also integrated in the metal housing. The necessary voltages for operation of the SDD elements are provided by one external power supply and are distributed *via* bond wires directly at the silicon chip. The complete system (*i.e.* housing of the SDD chip, power supply and amplifier and shaper electronics) was built at HASYLAB. The set-up of the further signal-processing chain is described in detail in §3.1.1 and is shown in Fig. 2 (without the Ortec 579 amplifier). No cooling was applied to the detector, which led to an SDD chip temperature of about 300 K.

2.3. SDD performance aspects: results and discussion

Results of the experiments are plotted in Fig. 3 for two detector temperatures, 293 K and 255 K.

The values of the FWHM were calculated using a Gaussian fit at the Zn K_{α} fluorescence line (8.6 keV). The values of the FWHM increase linearly with the number of incoming counts (slope 0.25×10^{-3} eV count⁻¹). In general an increase of the FWHM can be explained by electronics effects, *e.g.* uncertainties in the baseline-restore. At TCR ≈ 150 kcounts s⁻¹ it is found that FWHM ≈ 300 eV.

At lower temperatures the energy resolution becomes significantly better, and $\text{FWHM} < 300 \text{ eV}$ can be achieved up to very high count rates of about $400 \text{ kcounts s}^{-1}$ [similar to results by Strüder *et al.* (1997) and Lechner *et al.* (2001)]. Fig. 3 also shows that P/B decreases with increased TCR. The reasons for this behaviour have to be further investigated.

Results from the experiments on the seven-element SDD are shown in Fig. 4. It can be seen that the FWHM increases to $\sim 340 \text{ eV}$ at $150 \text{ kcounts s}^{-1}$ (with a slope of $\sim 0.6 \times 10^{-3} \text{ eV count}^{-1}$), which is not as good as that found for the single-pixel SDD (although for low count rates the performance is found to be better, *e.g.* $\text{FWHM} \simeq 250 \text{ eV}$ at $\text{TCR} \simeq 20 \text{ kcounts s}^{-1}$). It should be noted that the signal electronics for both SDD experiments consisted of different amplifiers. Thus the increase in the FWHM is not expected to be an effect of specific pulse processing electronics. From Fig. 4 one can also see

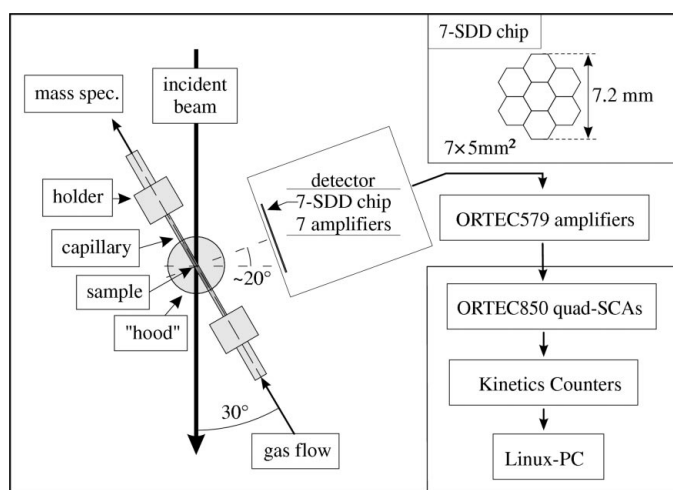


Figure 2 Schematic overview of the experimental set-up for *in situ* FLEXAFS studies: the seven-element silicon drift detector with electronics, and the *in situ* capillary cell with heating capabilities, gas supply and on-line gas analysis (for details see text). The inset shows a schematic view of the seven-element SDD chip.

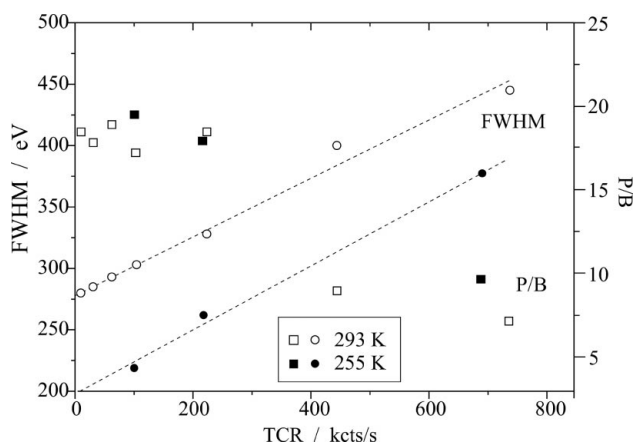


Figure 3 The energy resolution (FWHM) and the peak-to-background ratio (P/B) as a function of the total incoming count rate (TCR), measured for a single-pixel SDD. As a fluorescence test sample a Zn foil was irradiated with 10.5 keV photons. The data were acquired at two different temperatures, 293 K and 255 K.

that $\text{P/B} \simeq 4$ is decreased in comparison with the single-pixel detector. The lower performance of the seven-element SDD is due to a strong signal from elastically scattered photons contributing to the low-energy background B , due to operating the detector chip above room temperature ($\sim 300 \text{ K}$), and due to electronic effects in running a multi-element SDD instead of a single-element SDD. The voltages for operation of the seven-element SDD are generated by a common supply and then distributed to each element (see also §3.1.1). Slight electronic differences between the pixels cannot be excluded, and it was thus not possible to tune every pixel individually to its optimum performance. Hence a compromise between the detector elements had to be found.

Modern multipixel HP-Ge detector systems also show an increase of the FWHM with TCR. For instance, the 30-element HP-Ge presented by Farrow *et al.* (1998) exhibits a non-linearly increasing FWHM with an average slope of about $1 \times 10^{-3} \text{ eV count}^{-1}$ [calculated from the corresponding figures of Farrow *et al.* (1998) by averaging the slopes for a TCR interval of about $300 \text{ kcounts s}^{-1}$]. This increase is comparable with those found for the SDDs.

The weak dependencies $\text{FWHM}(\text{TCR})$ found for the SDDs also imply that the use of single-channel analyzers for detecting the fluorescence intensity of interest is not usually a problem for fluorescence XAFS (even if the SCA windows are fixed during an XAFS scan). Especially in the case of low-concentrated systems, TCR only changes by typically $10\text{--}20 \text{ kcounts s}^{-1}$ while crossing an absorption edge. This has negligible influence on the fluorescence XAFS spectrum because the FWHM of the discriminated fluorescence signal changes only slightly (*e.g.* for the seven-element SDD: $300 \text{ eV} \rightarrow 312 \text{ eV}$ for $90 \text{ kcounts s}^{-1} \rightarrow 110 \text{ kcounts s}^{-1}$ at $\text{Ni } K_{\alpha}$).

The results from the experiments on the single-pixel SDD demonstrate that its performance is good even at very high count rates. Both the energy resolution [see also *e.g.* Strüder *et al.* (1997), Strüder, Fiorini *et al.* (1998), Lechner *et al.* (2001)] and the peak-to-background ratio [see also *e.g.* Kappen, Tröger *et al.* (2001)] were found to be very high. The properties of the seven-element SDD appear to be slightly worse compared with the single-pixel SDD. However, they still meet very well the requirements for time-resolved fluorescence XAFS studies on low-concentrated samples, *e.g.* catalyst samples (*e.g.* Kappen *et al.*, 2001).

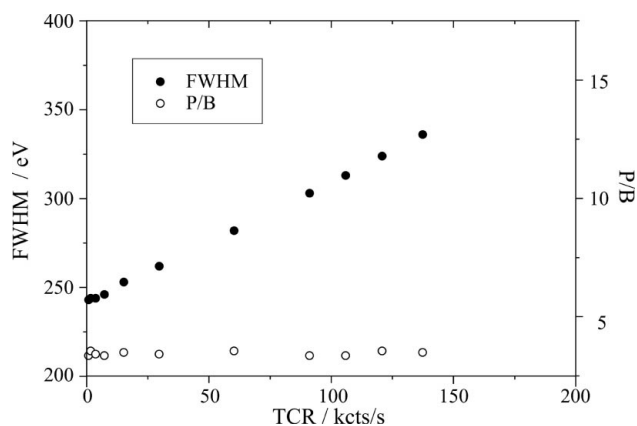


Figure 4 The energy resolution (FWHM) and the peak-to-background ratio (P/B) for the $\text{Ni } K_{\alpha}$ -fluorescence line ($E = 7.47 \text{ keV}$) as a function of the total incoming count rate (TCR), measured for a seven-pixel SDD. A sample consisting of 1.8 wt% Ni/7.1 wt% Mo/ Al_2O_3 served as a fluorescing object (irradiation with 12 keV photons).

3. Application of a multi-element SDD: investigation of low-concentrated catalysts

For catalysis research it is seldom sufficient to know the structural details of a catalyst before and after use. For a detailed understanding of the dynamic behaviour of a catalyst it is necessary to perform time-resolved studies under reaction conditions. XAFS has been demonstrated to be particularly useful in this respect (Clausen *et al.*, 1998; Iwasawa, 1996; Prins & Koningsberger, 1988). For catalysts containing the element of interest in low concentrations the fluorescence detection mode is the preferred tool, and the additional need of time resolution requires a detector which allows the processing of high count rates at good energy resolution.

In the following sections the experimental set-up and conditions for the investigation of catalyst samples by a multi-element SDD will be presented. We will also show examples of noble metal catalysts investigated *ex situ* and *in situ* at the Au L_{III} and the Pt L_{III} absorption edge. Gold catalysts are, for instance, known to oxidize carbon monoxide at low temperatures (Haruta, 1997; Valden *et al.*, 1998; Grunwaldt & Baiker, 1999), and platinum-based catalysts are used in hydrogenation/dehydrogenation and oxidation reactions (Ertl *et al.*, 1997). Usually the noble metal loading is low because of the high cost of the noble metal and in order to achieve a high dispersion.

3.1. Experimental

3.1.1. Beamline and detector set-up. Catalyst samples were investigated by fluorescence XAFS at the undulator beamline BW1 (Frahm *et al.*, 1995) at HASYLAB. An Si(111) double-crystal monochromator was used for the XAFS scans and the beam intensity was controlled using a MoStab as described above (see §2.2). The undulator was operated at a gap spacing that allowed energy scans without large changes in photon flux. The beam size at the sample position was fixed to 12 mm × 1 mm using a standard slit system.

The detector used for the experiments was the seven-element SDD introduced in §§1 and 2.3. Its signals were fed to filter amplifiers (ORTEC 579) inside the experimental hutch (see Fig. 2), providing pulses of 3 V amplitude at 10 keV photon energy. These signals could be transferred outside of the hutch without significant noise pick-up. For each detector pixel, two single-channel analysers (ORTEC Quad SCA 850) were used to discriminate the total SDD signals and the signals in the fluorescence line of interest, respectively. The TTL-output pulses from the SCAs were counted by Kinetics HEX-Counters (3610-L2A) mounted in a Camac crate. Beamline and electronics were controlled by a Linux PC. Additionally, multi-channel analyzer spectra could be recorded with an ADC/MCA module (LeCroy 3512/3588).

The distance between sample and detector was about 5 cm, which corresponds to a solid angle of $4\pi \times 0.02\%$ per pixel. As can be seen from Fig. 2, the detector was not placed exactly perpendicular to the beam axis ($\sim 20^\circ$). Owing to polarization effects, this leads to some increase of the total count rate by elastic scattering.

3.1.2. Data processing. The data acquired from each of the detector pixels were corrected for the dead time τ of the corresponding signal chain containing the detector pixel, amplifiers and the SCA. By irradiating a metal foil as fluorescence test sample, $\tau \simeq 700$ ns was found, where the paralyzable dead-time model (Knoll, 1979; Zhang *et al.*, 1992) was applied. After dead-time correction the spectra from the different detector pixels were added up using individual weighting factors, such that small weights are used for high background and/or low edge jump data, and *vice versa* for high-quality data. The weighting factor W was defined as the relative edge jump, $W := J/B$, where J is the edge jump calculated at the edge

position and B is the pre-edge background value. Per fluorescence XAFS scan, the different values of W for the different detector pixels were typically found to be very similar ($\pm 15\%$). It should be noted that W is only valid for spectra that exhibit statistical uncertainties, *i.e.* any systematic error is neglected.

Self-absorption was disregarded due to the low concentrations of the investigated elements.

3.1.3. Ex situ experiments. Samples were investigated at room temperature and in ambient air. The catalysts were pressed into pellets, each with a thickness of about 1 mm: 1 wt% Au on TiO₂, 700 ppm Au plus 400 ppm Pd on Al₂O₃, and 157 ppm Pt plus 3340 ppm Ru on Al₂O₃. The Au/TiO₂ sample was prepared by deposition of colloids [similar to Grunwaldt *et al.* (1999)] followed by drying at 323 K. For the AuPd/Al₂O₃ sample, Au(III) and Pd(II) precursors were deposited on the Al₂O₃ support and calcined at 383 K. The PtRu sample was prepared by adsorption of H₂PtCl₆ and RuCl₃ under similar conditions as the Au/TiO₂ sample and subsequent drying at 323 K.

The pellets were mounted such that their surface normal formed an angle of 45° – 60° with respect to the X-ray beam axis. Fluorescence XAFS scans were recorded around the Au and Pt L_{III} edges. Each scan (scan range $\Delta E \simeq 600$ eV) was recorded in less than 1 h.

3.1.4. In situ experiments. The *in situ* experiments were performed on a sample containing 0.3 wt% platinum and 0.5 wt% palladium in a matrix consisting of ~ 70 wt% Al₂O₃ and ~ 30 wt% zeolite. The powder (sieve fraction 75–125 μm) was loaded in a quartz glass capillary of outer diameter 1.0 mm and wall thickness 0.01 mm. The capillary served both as an *in situ* cell for fluorescence XAFS and as a reaction cell where the temperature (up to 773 K) and gas flow (in the ml min⁻¹ range) can be adjusted. Moreover, on-line gas analysis was performed by a mass spectrometer (Balzers Thermostar), similarly as in previous transmission XAFS experiments (Clausen *et al.*, 1991; Grunwaldt *et al.*, 2000). The capillary was mounted at a 30° angle with respect to the beam axis so that a sufficiently large sample volume could be illuminated (Fig. 2).

In the first step of the *in situ* experiment a fluorescence XAFS scan of the sample was recorded at room temperature. Then the sample was heated in hydrogen flow (2.5 ml min⁻¹) with a constant temperature ramp of 2.5 K min⁻¹ up to 573 K. During this treatment, fluorescence XANES spectra were taken in the near-edge region of the platinum L_{III} -edge ($\Delta E = 110$ eV, acquisition time 10 min per spectrum). At 573 K and after subsequently cooling the sample to room temperature, additional fluorescence XAFS scans were recorded ($\Delta E = 600$ eV, acquisition time $\simeq 45$ min).

In the second step of the *in situ* experiment the same sample was heated in a flow of 500 ppm SO₂ in air (2 ml min⁻¹) with a constant temperature ramp of 2.5 K min⁻¹ up to 653 K. Again, fluorescence XANES spectra were recorded in the near-edge region of the Pt L_{III} -edge while heating up, and finally fluorescence XAFS spectra were measured both at 653 K and at room temperature.

3.2. Results and discussion

3.2.1. Ex situ investigation of gold- and platinum-based catalysts.

Ex situ fluorescence XAFS spectra with the corresponding MCA spectra for the Au/TiO₂, AuPd/Al₂O₃ and PtRu/Al₂O₃ samples are shown in Figs. 5, 6 and 7, respectively. The MCA spectra in all three examples exhibit the fluorescence line of the element of interest to be well separated from the signals originating from matrix elements or elastically scattered photons. Note that in the case of the alumina supported catalysts no matrix signals can be observed, since Al $K_{\alpha,\beta}$ fluorescence radiation is too low in energy to be able to penetrate the ambient air and the window material of the detector. Minor fluor-

escence lines and/or lines of ambiguous origin are labelled in brackets. The fluorescence XAFS spectra exhibit relative noise amplitudes† of 10^{-2} – 10^{-3} , and therefore XAFS structures can be well extracted. After background removal using spline functions, Fourier transforms of the k^1 -weighted $\chi(k)$ -functions for the gold-containing samples were calculated ($k = 2.5$ – 12.0 \AA^{-1}). The results are depicted in Fig. 8(a).

The fluorescence XAFS spectrum of the gold-containing alumina sample (Fig. 6) exhibits a distinct white line which indicates that gold is in an oxidized state. The corresponding Fourier transform (Fig. 8a) reveals two major peaks at 1.7 Å and 3.2 Å. The comparison with transforms of reference spectra from metallic gold and from Au₂O₃ (Fig. 8b) indicates that the catalyst sample contains both metallic gold and gold in a higher oxidation state.

In contrast to this sample, the Au/TiO₂ catalyst does not contain gold in an oxidized state as indicated by the absence of a white line in

the fluorescence XAFS scan (Fig. 5). The corresponding Fourier transform supports this conclusion, because no contribution is found at 1.7 Å (Fig. 8a). This shows that the preparation process using colloidal gold deposition (Grunwaldt *et al.*, 1999) with subsequent mild drying results in metallic gold particles on the titania support.

Results obtained from the third sample (PtRu/Al₂O₃; Fig. 7) exhibit a pronounced white line, which indicates that platinum is not in the fully reduced state. When platinum catalysts are reduced, typically a decrease in the intensity of the white line can be observed (Bazin *et al.*, 1996, 1999).

The results demonstrate that good quality fluorescence XAFS spectra, using the seven-element SDD, can be obtained at concentrations as low as 100 ppm. They also show that the detector is well suited for time-resolved studies of the investigation of atoms incorporated in heavy matrices. This is not only due to its high-count-rate performance, but also because it is quite handy (no cooling system). Hence, it can be used in combination with a reaction cell (see §3.1.4), which allows structural changes to be followed *in situ* and even allows on-line gas monitoring, as it is important in the field of catalysis (Grunwaldt *et al.*, 2001). These properties and the current further

† The relative noise amplitude is defined as the statistical noise of a spectrum in an appropriate energy region above the absorption edge divided by the corresponding fluorescence intensity.

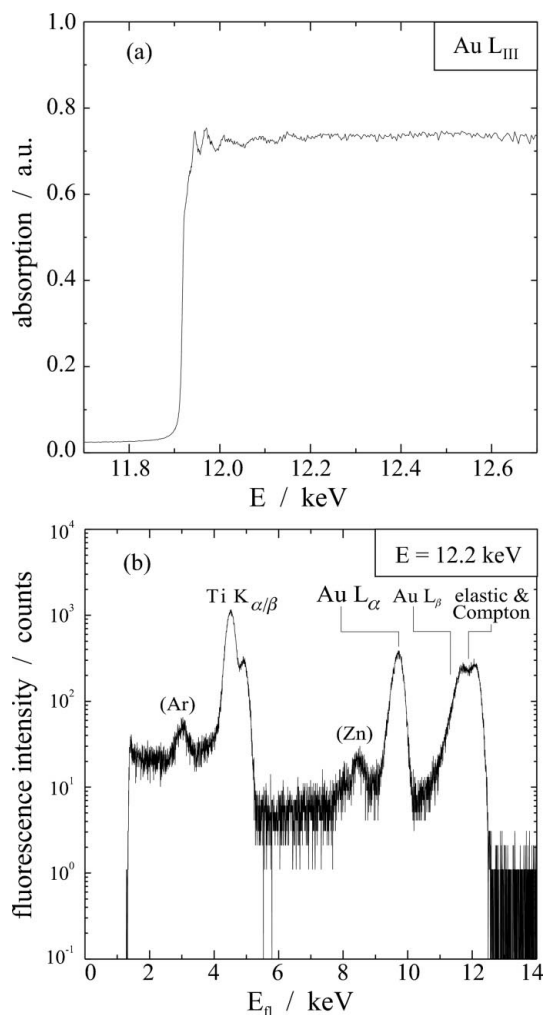


Figure 5
(a) *Ex situ* fluorescence XAFS at the Au L_{III}-edge of a catalyst consisting of 1 wt% Au on TiO₂. (b) The corresponding MCA spectrum recorded using an excitation energy of 12.2 keV. (Labels in brackets: Ar fluorescence from the ambient air, Zn fluorescence from impurities.)

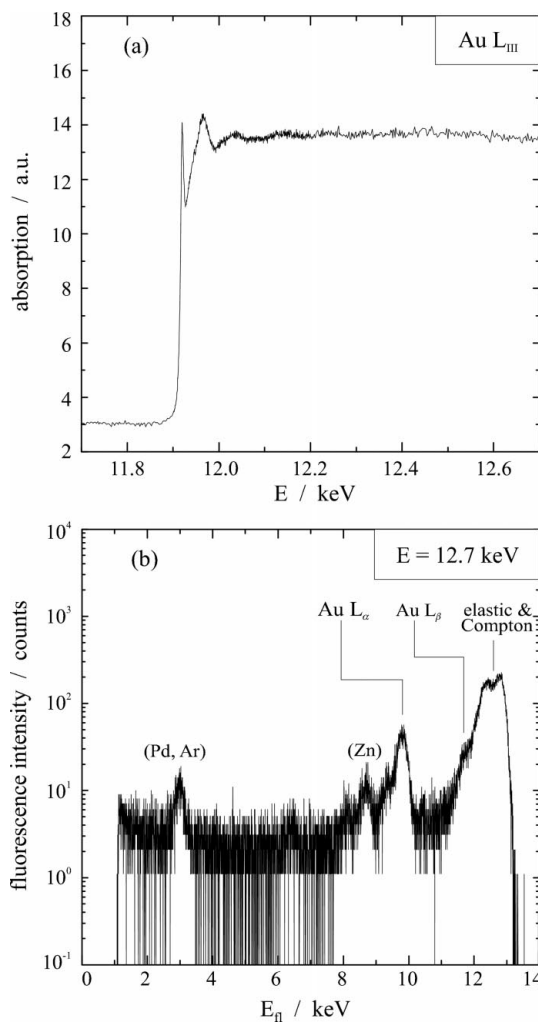


Figure 6
(a) *Ex situ* fluorescence XAFS at the Au L_{III}-edge of a catalyst consisting of 700 ppm Au and 400 ppm Pd on Al₂O₃. (b) Corresponding MCA spectrum recorded using an excitation energy of 12.7 keV. (Labels in brackets: Ar fluorescence from the ambient air and/or Pd fluorescence from the sample, Zn fluorescence from impurities.)

development of monolithic multi-element SDDs with even more pixels (Hansen & Tröger, 2000; Lechner *et al.*, 2001) show that SDDs are an interesting alternative to other fluorescence detectors [Lytle type, Si(Li), HP-Ge *etc.*]. As outlined in the *Introduction*, ongoing development in the field of Ge detectors also results in systems with high-count-rate performance and compact cooling (Farrow *et al.*, 1998; Derbyshire *et al.*, 1999) which are thus useful for similar applications as the SDDs.

Presently, most of the time-resolved XAFS experiments are performed in the transmission mode (Clausen *et al.*, 1998; Iwasawa, 1996; Prins & Koningsberger, 1988). The lower limit of concentration in solid samples is, however, typically found to be at about 1 wt% in the case of heavy matrix elements (Kappen *et al.*, 2001) and at about 1000 ppm for a light matrix (*e.g.* Brown *et al.*, 1988, and references therein). This also becomes obvious from Table 1, showing relative edge jumps $J_{r, \text{fluo}}$ and $J_{r, \text{transm}}$ of the XAFS scans on the three samples investigated *ex situ*. Hence, fluorescence XAFS is also a better alternative in this case.

The lowest concentration at which it is possible to record good quality fluorescence XAFS data depends on the experimental set-up,

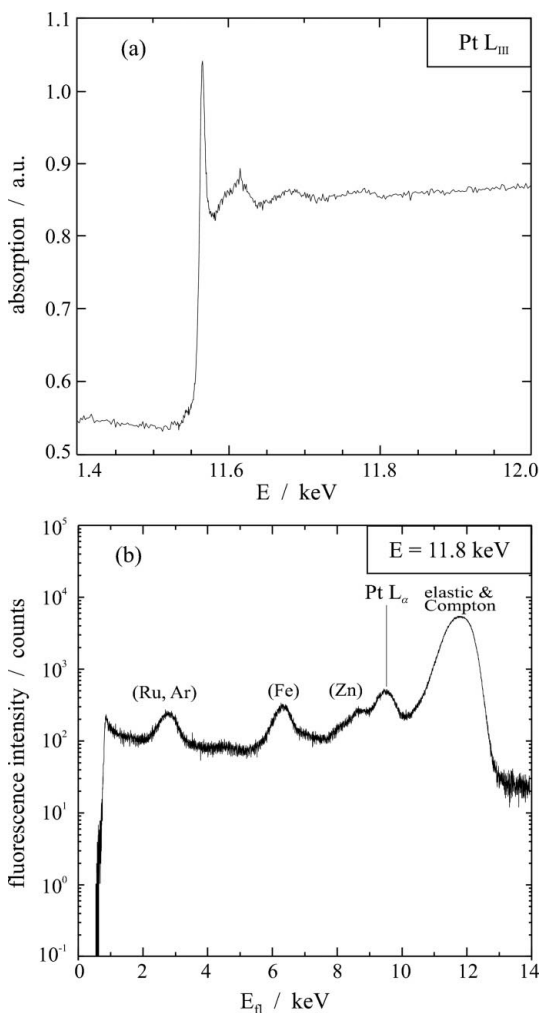


Figure 7
(a) *Ex situ* fluorescence XAFS at the Pt L_{III} -edge of a catalyst consisting of 157 ppm Pt and 3340 ppm Ru on Al_2O_3 . *(b)* Corresponding MCA spectrum recorded using an excitation energy of 11.8 keV. (Labels in brackets: Ar fluorescence from the ambient air and/or Ru fluorescence from the sample, Zn and Fe fluorescence from impurities.)

Table 1
 Relative edge jumps J_r for the *ex situ* investigated samples.

$J_r := J/B$, where J and B are defined in §3.1.1. $J_{r, \text{fluo}}$ is calculated from the fluorescence EXAFS spectra and $J_{r, \text{transm}}$ from transmission EXAFS data with absorption $\mu d = 1.5$.

Sample	$J_{r, \text{fluo}}$	$J_{r, \text{transm}}$
1 wt% Au on TiO_2	22.75	0.04
700 ppm Au on Al_2O_3	3.30	0.01
157 ppm Pt on Al_2O_3	0.55	0.002

the detection geometry and the matrix surrounding the element of interest. In the case of heavy matrix elements their fluorescence intensity dominates the total count rate at the detector. For samples with comparatively heavy matrix elements (*e.g.* Ti, V, Mn) a light filter foil (*e.g.* C or Al) placed between sample and detector can be used to reduce the fluorescence from the matrix atoms considerably, hence leading to a significant decrease in the total count rate. This may allow the total flux of primary photons on the sample to be increased, resulting in an increase of the count rate of the element of interest. The option of using light-element filters is especially interesting for the study of heavier elements, *e.g.* noble metals in a light matrix, where the filter is almost transparent for the fluorescence radiation from the metal atoms but opaque to the fluorescence from the matrix. Aluminium filters were successfully applied to investigate gold in MnO_2 (Grunwaldt *et al.*, 2002). Light-element filter foils are not

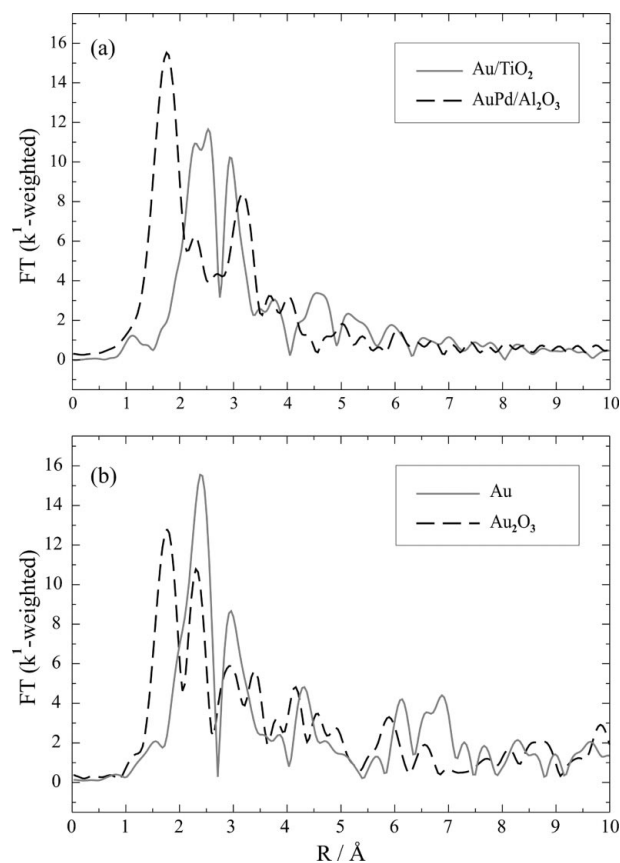


Figure 8
 Fourier transforms of *(a)* the fluorescence EXAFS spectra of the gold-containing catalysts (Au/ TiO_2 : full line; AuPd/ Al_2O_3 : dashed line), and of *(b)* transmission EXAFS data of a Au-foil reference (full line) and an Au_2O_3 reference (dashed line). Note that the distance scale is not corrected for the phase shift.

useful if the fluorescence lines from the matrix and the element of interest are close together.

It should be noted that the option of balancing the count rates from the matrix and the element of interest by the use of filters does not diminish the need for high-count-rate detectors. Such detectors are indispensable for applications at high-flux X-ray light sources, e.g. at undulator beamlines.

3.2.2. *In situ* studies of a platinum-based catalyst during reduction and oxidation. Figs. 9(a) and 9(b) show the XANES spectra recorded during the temperature-programmed reaction, i.e. the application of a linear heating ramp under the corresponding reaction conditions. Using a heating ramp of 2.5 K min^{-1} , in every 25 K interval a XANES spectrum was obtained. One can clearly see how the white line at the Pt L_{III} -edge decreases upon reaction in H_2 (indicating reduction of the Pt) and subsequently increases (indicating oxidation) upon treatment in SO_2/air at increasing temperature. The fluorescence XAFS spectrum after oxidation in SO_2/air is

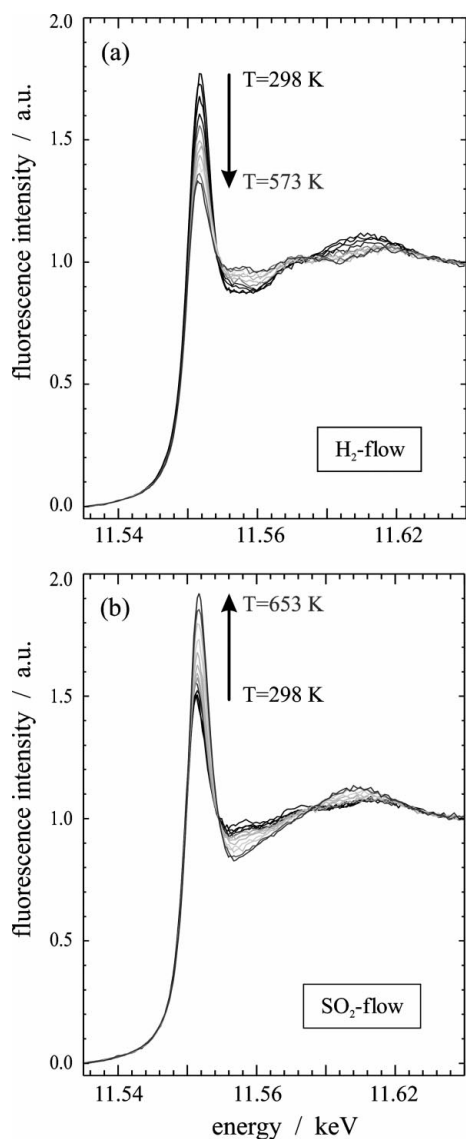


Figure 9
In situ XANES during reduction and oxidation of Pt in a PtPd/zeolite catalyst: (a) heating in H_2 -flow (2.5 ml min^{-1} , 2.5 K min^{-1}) and (b) heating in SO_2/air -flow (2.0 ml min^{-1} , 2.5 K min^{-1}). Each spectrum was recorded in about 10 min.

very similar to the starting spectrum before reduction in H_2 (not shown in a separate figure). The continuous decrease and increase of the white line during the *in situ* experiment reveals that, within the time resolution, both processes occur smoothly with no intermediate steps as, for example, observed for catalysts with low copper concentration (Kappen *et al.*, 2001; Yamagushi *et al.*, 2000). The reduction starts already at quite low temperatures ($<323 \text{ K}$). Similarly the oxidation proceeds smoothly, starting at a temperature below 373 K . Bazin *et al.* (1996, 1999) also studied the reduction of platinum by analysis of the white-line intensity. They found the reduction occurring above 423 K , proceeding rapidly in the beginning and going on more slowly until 573 K . The catalyst in this study seems to be reduced much easier, which can be due to, for example, the particle size and the preparation procedure. However, differences in the reaction cell geometry may also explain the discrepancies. This will be studied in more detail in the future.

4. Conclusion

In the present study it was shown that multi-element silicon drift detectors with an integrated JFET are a very good tool for time-resolved *in situ* fluorescence XAFS studies on elements present in low concentrations in catalysts. A fluorescence XAFS set-up including a seven-element SDD and an *in situ* cell with gas supply and on-line gas analysis was developed for these purposes. Detector operation without cooling and at a total count rate of up to more than $100 \text{ kcounts s}^{-1}$ per element is possible. Even under these conditions the energy resolution is sufficient to separate the fluorescence lines of most elements encountered in catalysts.

The *in situ* reduction and oxidation of a zeolite-supported catalyst containing only 0.3 wt% platinum could easily be followed by this technique. Owing to the detector properties, fluorescence XANES spectra ($\Delta E = 100 \text{ eV}$) with good statistical quality (relative noise 10^{-2}) could be obtained. Within the time resolution of 10 min per scan, the reduction and oxidation of platinum occurred smoothly, as revealed by the decrease and increase of the white line. Thus, fluorescence XAFS using the *in situ* set-up can provide short-range-order information of a catalyst simultaneously to its catalytic properties.

Furthermore, results from *ex situ* fluorescence EXAFS investigations of low-concentrated gold and platinum catalysts on alumina and titania supports were obtained. The recorded spectra are of sufficient quality (relative noise $\sim 10^{-3}$) to allow Fourier transforms and quantitative analysis. This made it possible to distinguish between oxidation states of gold in samples prepared by different preparation modes. It appears that under typical experimental conditions concentrations of the element of interest as low as 100 ppm can be measured by fluorescence XAFS, using a multi-element SDD.

Further applications and improvement of fluorescence XAFS in combination with on-line catalysis will benefit from the current development of a 61-element SDD. This detector will give X-ray spectroscopy new possibilities, especially in connection with high-photon-flux light sources like undulator beamlines.

Experimental assistance from A. Kjersgaard and S. Rokni is gratefully acknowledged. We also would like to thank KETEK GmbH and MPI-Halbleiterlabor, Munich, for providing the silicon drift detector chips, for general support and for the cooperation within which the data for Fig. 3 were recorded. Also financial support by Dansync is gratefully acknowledged (JDG and BSC).

References

- Bazin, D., Dexpert, H. & Lynch, J. (1996). *X-ray Absorption Fine Structure for Catalysts and Surfaces*, edited by Y. Iwasawa. Singapore: World Scientific.
- Bazin, D., Dexpert, H., Lynch, J. & Bournonville, P. (1999). *J. Synchrotron Rad.* **6**, 465–467.
- Brown, G. E., Calas, G., Waychunas, G. A. & Petiau, G. (1988). *Rev. Mineral.* **18**, 431–512.
- Brown, G. E., Farges, F. & Calas, G. (1995). *Rev. Mineral.* **32**, 317–410.
- Chun, W.-J., Tanizawa, Y., Shido, T., Iwasawa, Y., Nomura, M. & Asakura, K. (2001). *J. Synchrotron Rad.* **8**, 168–172.
- Clausen, B. S., Steffensen, G., Fabius, B., Villadsen, J., Feidenhans'l, R. & Topsøe, H. (1991). *J. Catal.* **132**, 525–535.
- Clausen, B. S., Topsøe, H. & Frahm, R. (1998). *Adv. Catal.* **42**, 315.
- Derbyshire, G., Cheung, K.-C., Sangsingkeow, P. & Hasnain, S. S. (1999). *J. Synchrotron Rad.* **6**, 62–63.
- Ertl, G., Knötzinger, H. & Weitkamp, J. (1997). Editors. *Handbook of Heterogeneous Catalysis*, Vols. 3–5. Weinheim: VCH.
- Farrow, R. C., Headspith, J., Dent, A. J., Dobson, B. R., Bilsborrow, R. L., Ramsdale, C. A., Stephenson, P. C., Brierley, S., Derbyshire, G. E., Sangsingkeow, P. & Buxton, K. (1998). *J. Synchrotron Rad.* **5**, 845–847.
- Frahm, R. (1989). *Rev. Sci. Instrum.* **60**, 2515–2518.
- Frahm, R., Weigelt, J., Meyer, G. & Materlik, G. (1995). *Rev. Sci. Instrum.* **66**, 1677–1680.
- Gatti, E. & Rehak, P. (1984). *Nucl. Instrum. Methods Phys. Res. A*, **225**, 608–614.
- Gautier, Ch., Goulon, J., Moguiline, E., Rogalev, A., Lechner, P., Strüder, L., Fiorini, C., Longoni, A., Sampietro, M., Besch, H., Pfitzner, R., Schenk, H., Tafelmeier, U., Walenta, A., Misiakos, K., Kavadias, S. & Loukas, D. (1996). *Nucl. Instrum. Methods Phys. Res. A*, **382**, 524–532.
- Gregor, R. E., Pingitore, N. E. Jr & Lytle, F. W. (1997). *Science*, **275**, 1452–1454.
- Grunwaldt, J.-D. & Baiker, A. (1999). *J. Phys. Chem. B*, **103**, 1002.
- Grunwaldt, J.-D., Kappen, P., Basini, L. & Clausen, B. S. (2001). *Catal. Lett.* **78**, 13–21.
- Grunwaldt, J.-D., Kappen, P., Hammershøi, B. S., Tröger, L. & Clausen, B. S. (2001). *J. Synchrotron Rad.* **8**, 572–574.
- Grunwaldt, J.-D., Kappen, P., Tröger, L. & Clausen, B. S. (2002). To be published.
- Grunwaldt, J.-D., Kiener, Ch., Wögerbauer, C. & Baiker, A. (1999). *J. Catal.* **181**, 223–232.
- Grunwaldt, J.-D., Molenbroek, A. M., Topsøe, N.-Y., Topsøe, H. & Clausen, B. S. (2000). *J. Catal.* **194**, 452–460.
- Hansen, K. & Tröger, L. (2000). *IEEE Trans. Nucl. Sci.* **47**, 2748.
- Haruta, M. (1997). *Catal. Today*, **36**, 153.
- HASYLAB (2001). *X-ray Absorption Spectroscopy, In Situ Experiments, High-Energy Applications*, http://www-hasyllab.desy.de/facility/experiment_al_stations/stations/X1.htm.
- Iwasawa, Y. (1996). *X-ray Absorption Fine Structure for Catalysts and Surfaces*, Vol. 2. Singapore: World Scientific.
- Jaklevic, J., Kirby, J. A., Klein, M. P., Robertson, A. S., Brown, G. S. & Eisenberger, P. (1977). *Solid State Commun.* **23**, 679–682.
- Kappen, P., Grunwaldt, J.-D., Hammershøi, B. S., Tröger, L. & Clausen, B. S. (2001). *J. Catal.* **198**, 56–65.
- Kappen, P., Tröger, L., Hansen, K., Reckleben, Ch., Lechner, P., Strüder, L. & Materlik, G. (2001). *Nucl. Instrum. Methods Phys. Res. A*, **467/468**, 1163–1166.
- Knoll, G. F. (1979). *Radiation Detection and Measurement*, Section D. New York: Wiley.
- Krolzig, A., Materlik, G., Swars, M. & Zegenhagen, J. (1984). *Nucl. Instrum. Methods Phys. Res.* **219**, 430.
- Lechner, P., Andricke, L., Finedeis, N., Hauff, D., Holl, P., Kemmer, J., Klein, P., Lutz, G., Meidinger, N., Pinotti, E., Richter, R., Strüder, L. & Zanthier, C. v. (1993). *Nucl. Instrum. Methods Phys. Res. A*, **326**, 284–289.
- Lechner, P., Eckbauer, S., Harmann, R., Kirsch, S., Hauff, D., Richter, R., Soltau, H., Strüder, L., Fiorini, C., Gatti, E., Longoni, A. & Sampietro, M. (1996). *Nucl. Instrum. Methods Phys. Res. A*, **377**, 346–351.
- Lechner, P., Fiorini, C., Hartmann, R., Kemper, J., Krause, N., Leutenegger, P., Longoni, A., Soltau, H., Stötter, D., Strüder, L. & Weber, U. (2001). *Nucl. Instrum. Methods Phys. Res. A*, **458**, 281–287.
- Lépy, M. C., Campbell, J. L., Laborie, J. M., Plagnard, J., Stemmler, P. & Teesdale, W. J. (1999). *Nucl. Instrum. Methods Phys. Res. A*, **422**, 428–432.
- Leutenegger, P., Longoni, A., Fiorini, C., Strüder, L., Kemmer, J., Lechner, P., Sciuti, S. & Caesareo, R. (2000). *Nucl. Instrum. Methods Phys. Res. A*, **439**, 458–470.
- Lytle, F. W., Gregor, R. B., Sandstrom, D. R., Marques, E. C., Wong, J., Spiro, Cl., Huffman, G. F. & Huggins, F. E. (1984). *Nucl. Instrum. Methods Phys. Res. A*, **226**, 542–548.
- Manceau, A., Boisset, M. C., Sarret, G., Hazemann, J. L., Mench, M., Cambier, P. & Prost, R. (1996). *Environ. Sci. Technol.* **30**, 1540–1552.
- Prins, R. & Koningsberger, D. C. (1988). *X-ray Absorption: Principles, Applications, Techniques of EXAFS, SEXAFS and XANES*, Vol. 381. New York: Wiley.
- Sankar, G., Thomas, J. M., Rey, F. & Greaves, G. N. (1995). *J. Chem. Soc. Chem. Commun.* pp. 2549–2550.
- Shannon, I. J., Maschmeyer, T., Sankar, G., Thomas, J. M., Oldroyd, R. D., Sheehy, M., Madill, D., Waller, A. M. & Townsend, R. P. (1997). *Catal. Lett.* pp. 23–27.
- Shannon, I. J., Rey, F., Sankar, G., Thomas, J. M., Maschmeyer, T., Waller, A. M., Palomares, A. E., Corma, A., Dent, A. J. & Greaves, G. N. (1996). *J. Chem. Soc. Faraday Trans.* **92**, 4331–4336.
- Strüder, L. (2000). *Nucl. Instrum. Methods Phys. Res. A*, **454**, 73–113.
- Strüder, L., Eckbauer, S., Hartmann, R., Hauff, D., Holl, P., Kemmer, J., Lechner, P., Meidinger, N., Richter, R., Soltau, H., Zanthier, C.v., Fiorini, C., Gatti, E., Longoni, A. & Sampietro, M. (1997). *J. Phys. IV France*, **7(C2)**, 21–297.
- Strüder, L., Fiorini, C., Gatti, E., Hartmann, R., Holl, P., Krause, N., Lechner, P., Longoni, A., Lutz, G., Kemmer, J., Meidinger, N., Popp, M., Soltau, H. & Weber, U. & Zanthier, C. v. (1998). *J. Synchrotron Rad.* **5**, 268–274.
- Strüder, L., Lechner, P. & Leutenegger, P. (1998). *Naturwissenschaften*, **85**, 539–543.
- Strüder, L., Meidinger, N., Kemmer, J., Lechner, P., Leutenegger, P., Soltau, H., Eggert, F., Rohde, M. & Schulein, T. (1999). *Microsc. Microanal.* **4**, 622–631.
- Thomas, J. M., Greaves, G. N., Sankar, G., Wright, P. A., Chen, J., Dent, A. J. & Marchese, L. (1994). *Angew. Chem. Int. Ed. Engl.* **33**, 1871–1873.
- Valden, M., Lai, X. & Goodman, D. W. (1998). *Science*, **281**, 1647.
- Yamaguchi, A., Shido, T., Inada, Y., Kongure, T., Asakura, K., Nomura, M. & Iwasawa, Y. (2000). *Catal. Lett.* **68**, 139.
- Zhang, K., Rosenbaum, G. & Bunker, G. (1992). *J. Appl. Phys.* **32**, 147–149.